SF 298 MASTER COPY KEEP THIS COPY FOR REPRODUCTION PURPOSES

REPORT DOCUMENTATION PAGE

Form Approved OMB NO. 0704-0188

1. AGENCY USE ONLY *(Leave blank)*	2. REPORT DATE	3. REPORT TYPE AND DATES COVERED
	Aug 21, 1997	Final Progress Report 9/15/92 - 9/14/96

4. TITLE AND SUBTITLE

Ultrafast photochromic sol-gel glasses & fiber optic sensors

5. FUNDING NUMBERS

DAAL03-92-G-0399

6. AUTHOR(S)

Eric L. Chronister

7. PERFORMING ORGANIZATION NAMES(S) AND ADDRESS(ES)

Department of Chemistry
University of California
Riverside, CA 92521

8. PERFORMING ORGANIZATION REPORT NUMBER

9. SPONSORING / MONITORING AGENCY NAME(S) AND ADDRESS(ES)

U.S. Army Research Office
P.O. Box 12211
Research Triangle Park, NC 27709-2211

10. SPONSORING / MONITORING AGENCY REPORT NUMBER

11. SUPPLEMENTARY NOTES

The views, opinions and/or findings contained in this report are those of the author(s) and should not be construed as an official Department of the Army position, policy or decision, unless so designated by other documentation.

12a. DISTRIBUTION / AVAILABILITY STATEMENT

Approved for public release; distribution unlimited.

19971204 072

13. ABSTRACT *(Maximum 200 words)*

Organically doped sol-gel glasses have been investigated as fast response photochromic materials and as novel cladding materials for intrinsic fiber-optic chemical sensors. The following investigations are discussed: (1) Time-resolved spectroscopic measurements of fast optical energy transfer and trapping in organically doped glasses as a probe of the spatial distribution of chromophores within porous sol-gel matrices; (2) Picosecond photon echo measurements of homogeneous dephasing have been utilized as a probe of chromophore-host interactions; (3) Neutron diffraction measurements (small angle and quasi elastic) have been utilized to probe the local pore structure of sol-gel matrices; (4) Optical limiting based on fast photophysical processes in organic chromophores doped in sol-gel hosts; and (5) Time-resolved detection of intrinsic sol-gel clad fiber-optic chemical sensors. Optical energy transfer in organically doped sol-gel glasses have been investigated by time-resolved fluorescence depolarization measurements and analyzed in terms of the spatial distribution of chromophores in porous xerogel glasses. Picosecond photon echo measurements of the temperature dependent homogeneous dephasing rate of organically doped inorganic sol-gel glasses have probed irreversible low frequency dynamics of the sol-gel environment. And, intrinsic sol-gel clad fiber-optic chemical sensors have been demonstrated utilizing time-resolved optical detection of multiplexed sensors along fiber-optic waveguides.

14. SUBJECT TERMS

Sol-Gel Glass, Electronic Energy Transfer, Fiber-Optic, Chemical Sensor

15. NUMBER IF PAGES

25

16. PRICE CODE

17. SECURITY CLASSIFICATION OR REPORT	18. SECURITY CLASSIFICATION OF THIS PAGE	19. SECURITY CLASSIFICATION OF ABSTRACT	20. LIMITATION OF ABSTRACT
UNCLASSIFIED	UNCLASSIFIED	UNCLASSIFIED	UL

NSN 7540-01-280-5500

Standard Form 298 (Rev. 2-89)
Prescribed by ANSI Std. 239-18
298-102

ULTRAFAST PHOTOCHROMIC SOL-GEL GLASSES & FIBER OPTIC SENSORS

FINAL REPORT

ERIC L. CHRONISTER

AUGUST 18, 1997

U.S. ARMY RESEARCH OFFICE

GRANT NUMBER: DAALO3-92-G-0399

UNIVERSITY OF CALIFORNIA AT RIVERSIDE
RIVERSIDE, CA 92521

Table of Contents

LIST OF ILLUSTRATIONS

A. Statement of the Problem

This work has focused on utilizing sol-gel glasses as a new matrix for fast response optical materials and as a novel porous cladding material for intrinsic fiber-optic chemical sensors. The recent and continuing progress in the development of high intensity ultrashort laser sources and fiber-optic advances provides a fertile environment for these efforts. The goal of this project has been to develop and investigate "smart" optical materials based on optical energy transfer and relaxation processes in organically doped sol-gel glasses, as well as development of sol-gel clad fiber optic chemical sensors. A detailed understanding of the basic structure, chromophore dynamics, and photophysics of organically doped sol-gel glasses is desirable given the array of proposed applications for these novel materials (e.g. fluorescent planar concentrators [1] [2], solid state dye laser materials [3][4], optical data storage media [5], nonlinear optical materials [6], environmental impurity sensors [6], etc.). Sol-gel glasses hold promise as versatile nonlinear optical materials since they can solvate a wide variety of chromophores at high concentrations and the porous nature of the medium permits diffusion of analyte species. The sol-gel materials can be prepared chemically at room temperature by the hydrolysis of a variety of metal alkoxides, and thin films are easily produced by dip coating or spin casting [7]. Dried gels result in rigid xerogel glass matrix with considerable porosity(~50% void volume) [8] that can be controlled as a means of altering the index of refraction and/or the diffusion of analyte species.

B. Summary of Important Results

The methods for incorporating organic molecules into xerogel glass matrices have been well documented [9-11]. In addition, these materials have been developed or proposed as new solid-state laser materials [12-15], solar planar concentrators [16,17], chemical sensors [18], as well as optical limiting [19], and optical storage devices [20]. The growing interest in the optical applications of doped xerogels [21-23] further motivates our efforts to understand the spatial distribution of chromophores in xerogel glasses and how this distribution gives rise to the observed electronic energy transfer and trapping dynamics.

1. Fast Optical Energy Transfer and Trapping in Doped Sol-Gel Glasses

Sol-gel glasses can be doped at relatively high concentrations with minimal aggregation since gelation of the solution occurs before drying and shrinkage of the matrix. The resulting organically doped sol-gel glass films can have high chromophore concentrations with correspondingly fast optical energy transfer processes. Furthermore, time-resolved depolarization measurements have been used to probe the rate of electronic energy transfer and the spatial distribution of chromophores in organically doped sol-gel glasses. In the absence of rotational diffusion, fluorescence depolarization is a direct measure of electronic energy transfer between chromophores [24-26]. Since the rate of dipolar energy transfer is sensitive to the proximity of neighboring molecules (i.e. rate~r^{-6}), time-resolved fluorescence anisotropy measurements have been used to probe the spatial distribution of dopants [24] in silicate and aluminosilicate sol-gel glasses.

Time-resolved fluorescence lifetime and depolarization measurements have been used to investigate electronic excitation energy transfer and trapping in doped aluminosilicate sol-gel glasses. At low chromophore concentrations donor-donor electronic energy transfer is dominant, however, at higher concentrations energy trapping can be significant. Concentration dependent dynamics indicate dimer-like trap species and a nearly isotropic distribution of chromophores within the porous xerogel matrix. A comparison of wet gels versus porous xerogel glasses indicates that energy traps exist in the gel and that the number of traps does not significantly increase during formation of the (20 times) higher concentration xerogel glass. [25b]

In the absence of trap emission, the probability that energy is transferred from a donor to a trap can be probed experimentally by the total donor fluorescence intensity $I(t)$,

$$I(t) = I_o \exp(-t / \tau_D) \cdot G_{DT}^{s}(t) = I_o \exp(-t / \tau_D) \cdot \exp(-\alpha_{DT}\sqrt{t})$$

where t_D is the donor fluorescence lifetime in the absence of traps, and the non-exponential decay term is due to trapping of the donor excitation. [26,27]

Although donor-donor energy transfer does not affect the fluorescence intensity, it does give rise to depolarization of the fluorescence. Specifically, the probability of donor-donor transfer can be probed by measurement of the time-resolved fluorescence anisotropy *r(t)*,

$$r(t) = \frac{I_{\parallel}(t) - I_{\perp}(t)}{I_{\parallel}(t) + 2I_{\perp}(t)} = r_o \cdot G^s_{DD}(t) = r_o \exp(-\alpha_{DD}\sqrt{t})$$

where $I_{\parallel}(t)$ and $I_{\perp}(t)$ represent the time-resolved intensities of the fluorescence polarized parallel and perpendicular with respect to the polarization of the excitation pulse, and where α_{DD} is the donor-donor energy transfer parameter. When the excitation and emission transition dipole moments of the donor are parallel, r_o=*0.4* for an orientationally random chromophore distribution.

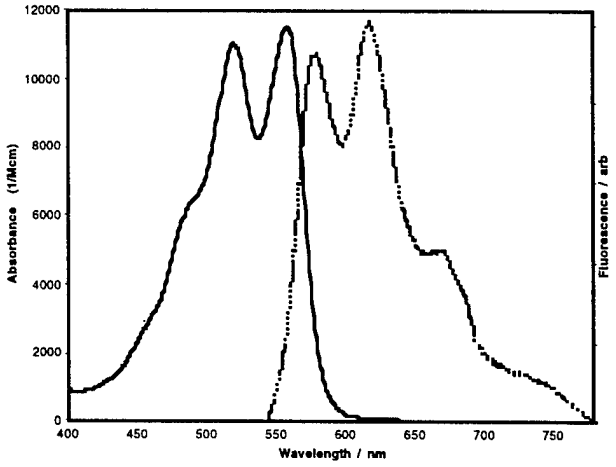

Fig. 1.1. Absorption spectrum (solid line) and emission spectrum (dashed line) of 0.005 M Q in an aluminosilicate xerogel. The absorption maxima are at 518 and 556 nm (e_{max} = 11600 $M^{-1}cm^{-1}$). The spectral overlap yields an orientationally averaged critical radius R_0 = 3.5 ± 0.4 nm.

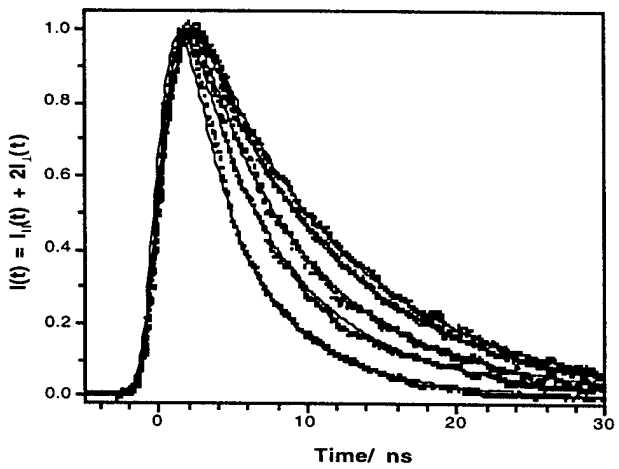

Fig. 1.2. Time-resolved fluorescence intensity I(t) decays for Q doped aluminosilicate xerogels at concentrations of 5.0 x10^{-4}, 1.1 x10^{-2}, 1.5 x10^{-2}, 2.0 x10^{-2}, and 2.7 x10^{-2} M. The solid curves represent convolutions of the instrument response with the above equation.

Although the absorption and emission spectra remained unchanged at higher Q concentrations, an increase in the Q-Al fluorescence decay rate was observed, as shown in **fig. 1.2**. The faster fluorescence decay rates suggest that trapping of the excitation energy occurs at higher Q concentrations. The fluorescence intensity decay at high Q concentrations is fit by the product of an exponential donor relaxation term and a concentration dependent nonexponential donor-trap energy transfer term. The donor fluorescence lifetime at low Q concentration (i.e. in the absence of trapping) was measured to be t_D = 10.3 ±0.5 ns.

In addition to energy trapping, energy transfer between donor molecules can be probed by the fluorescence anisotropy *r(t)* . Since the time-resolved anisotropy is proportional to the probability that the initially excited donor molecules remain excited at a time t after excitation, concentration dependent measurements of *r(t)* yield the donor-donor energy transfer parameter α_{DD}. **Fig. 1.3** shows an increase in the anisotropy decay rate with increasing chromophore concentration. Furthermore, energy

transfer/trapping was observed to be nearly dispersionless for different excitation energies (e.g. 560 nm → 572 nm), indicating that the absorption and emission spectra are primarily homogeneously broadened at room temperature.

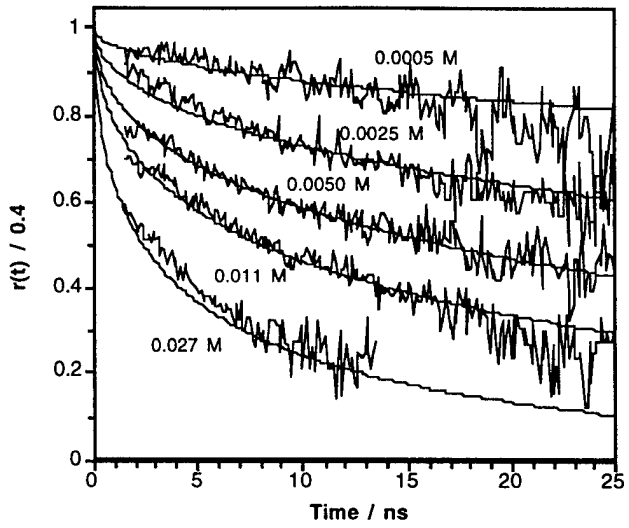

Fig. 1.3. Time-resolved anisotropy *r(t)* decays for Q doped aluminosilicate xerogels at Q concentrations of 5.0×10^{-4}, 2.5×10^{-3}, 5.0×10^{-3}, 1.1×10^{-2}, and 2.7×10^{-2} M. The solid lines are calculated fits of the data.

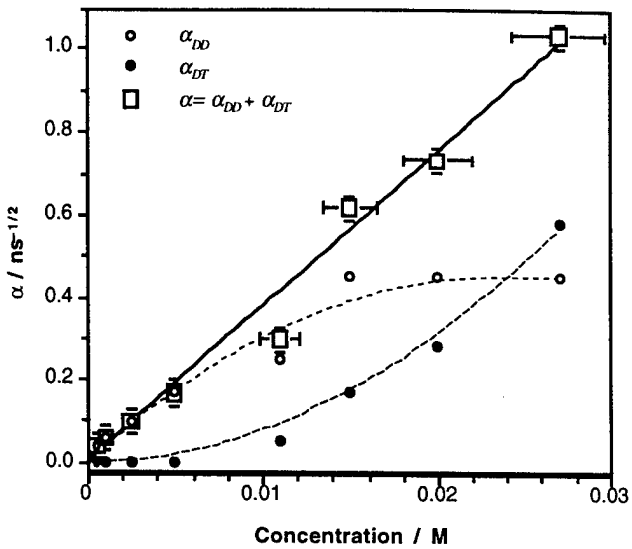

Fig. 1.4. The energy transfer and energy trapping for Q in aluminosilica. The donor–donor α_{DD} (open circles) and donor–trap α_{DT} (filled circles) energy transfer parameters are plotted versus concentration. α_{DT} increases quadratically with Q concentration, as shown by the dashed line fit to $\alpha_{DT} = 744\ ns^{-1/2}M^{-2}\ [Q]^2$. In contrast, the donor–donor transfer parameter α_{DD} does not increase above 1.5×10^{-2}M (dotted line). The sum of the energy transfer and trapping parameters $\alpha=\alpha_{DD}+\alpha_{DT}$ (squares) increases linearly with concentration, corresponding to a donor critical radius $R_o = 3.55$ nm.

The energy transfer results summarized in **fig. 1.4** suggest that at high Q concentrations the aluminosilicate xerogel glasses contain traps that are not evident in the absorption and emission spectra. Furthermore, the quadratic dependence of α_{DT} on the Q concentration suggests that the traps are ground state dimers of Q-Al. The open squares in **fig. 1.4** are obtained by summing the experimentally observed energy transfer and trapping parameters, i.e. $\alpha = \alpha_{DD} + \alpha_{DT}$ (open squares) and they compare favorably with the solid line determined from the donor spectral overlap. This correspondence lends support to the simple trapping model in which the dominant trap is an isotropically distributed Q-Al dimer species.

Optical energy transfer and trapping in 9-aminoacridine doped sol-gel glasses. 9-aminoacridine (9AA) doped sol-gel glasses were utilized to investigate the role that guest host interactions play in determining both the spatial distribution of chromophores and the resulting optical energy dynamics. [28] Specifically, time-resolved polarized fluorescence measurements of 9AA doped into silicate xerogel (SX) and aluminosilicate xerogel (ASX) glasses were used to probe energy transfer within the xerogel matrix. At low concentrations the dynamics are dominated by donor-donor

energy transfer processes, however, energy trapping by aggregate species is observed at higher concentrations. In addition, a comparison of the anisotropy decay rates and the critical radius obtained from the spectral overlap indicates a significant excluded volume within the xerogel matrix. An unresolved fast anisotropy decay component for 9AA doped ASX suggests a non-random spatial distribution of chromophores within the occupied restricted volume of the ASX matrix.

The absorption and emission spectra of an aluminosilicate xerogel sample doped with 9AA at a concentration of $1x10^{-3}$ M are shown in **Fig. 1.5**. Except for a typical solution to xerogel red-shift, and the slightly broader features in the xerogel, the absorption spectra closely matched those reported for dilute solutions of 9AA in water [29-31], glycerol [32], propylene glycol [33] and stretched poly(vinyl alcohol) films [33b]. For all dopant concentrations in both matrices, the emission spectra were identical to that obtained for a $1x10^{-5}$M 9AA aqueous solution. The absorption and emission spectra did not show any spectral features that could be attributed to dimers, excimers, aggregates and/or protonated species that have been reported for 9AA concentrations above 10^{-2}M in solution [29,30]. Since little spectral change is observed when 9AA is incorporated into SX and ASX, this suggests that the chromophore remains unchanged during the sol to xerogel transition.

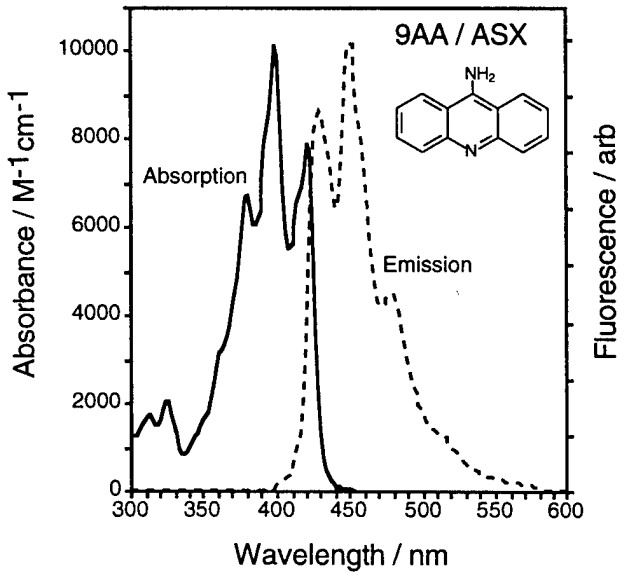

Fig. 1.5. Absorption spectrum (solid line) and emission spectrum (dashed line) of 0.001 M 9-aminoacridine doped aluminosilicate xerogel (9AA/ASX). The absorption maxima are at 382, 402, and 424 nm. The spectral overlap integral yields an orientationally averaged critical radius $R_o = 2.6 \pm 0.1$ nm.

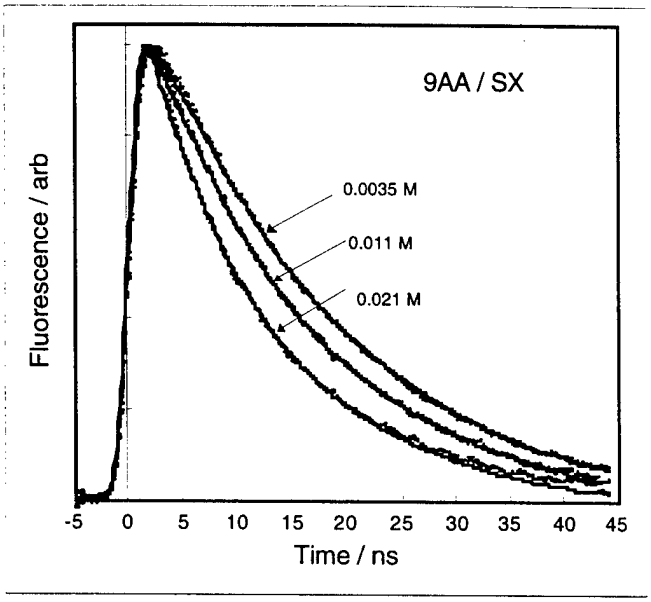

Fig. 1.6. Time resolved fluorescence intensity I(t) decay for 9-aminoacridine doped silica xerogel (9AA/SX). Typical traces for dopant concentrations of 0.0035, 0.011, and 0.021 M are shown. The solid curves are calculated fits.

Time Resolved Fluorescence Spectra. Concentration dependent fluorescence decays for 9AA/SX are shown in **Fig. 1.6**. At concentrations below $5x10^{-3}$M a single exponential fluorescence decay is observed, yielding a fluorescence lifetime of $t_D = 15.7 \pm 0.5$ ns. At dopant concentrations above 7×10^{-3} M faster fluorescence decays were observed. The effect of trapping (open squares) becomes significant above a 9AA concentration of 0.09 M in both SX and ASX, and a rapid increase in the rate of donor-trap energy transfer is observed in both the SX (fig. 1.8) and ASX (fig. 1.9) matrices at higher 9AA concentrations, with a corresponding leveling off of the donor-donor

parameter. For the 9AA/ASX system (not shown), the fluorescence decay rate increased at 9AA concentrations above 6 x 10^{-3} M.

The concentration dependent trapping parameter for 9AA/SX shown in fig. 1.8 increases nearly quadratically with 9AA concentration as α_{DT} = 484 $ns^{-1/2}M^{-2}$ • $[9AA]^2$ (dotted line), which suggests the formation of a dimer trap species. In comparison, the energy trapping in 9AA/ASX, shown in fig. 1.9, has a stronger concentration dependence, fit by $\alpha_{DT} = 5.2x10^4$ $ns^{-1/2}M^{-3}$ • $[9AA]^3$ (dotted line), possibly indicating the formation of larger aggregate species. The energy trapping results summarized in figs 1.8 & 1.9 show that when either of the SX and ASX xerogel glasses are doped at 9AA concentrations greater than 0.09 M, energy traps are formed which are not clearly detected in the absorption and/or emission spectra.

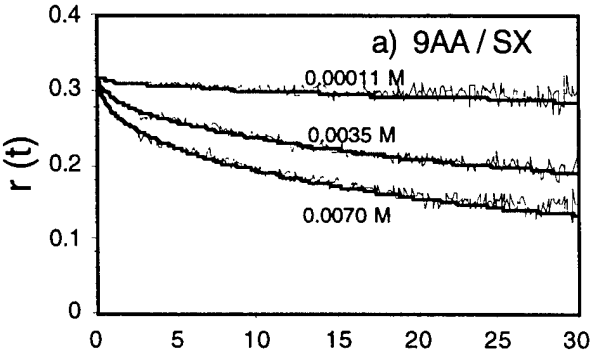

Fig. 1.7a. Time resolved anisotropy *r(t)* decays for 9-aminoacridine doped silicate silicate xerogels (9AA/SX) with dopant concentrations of 1.1x10^{-4}, 3.5x10^{-3}, and 7.0x10^{-3} M. The solid curves are fits of the data with r_o = 0.32.

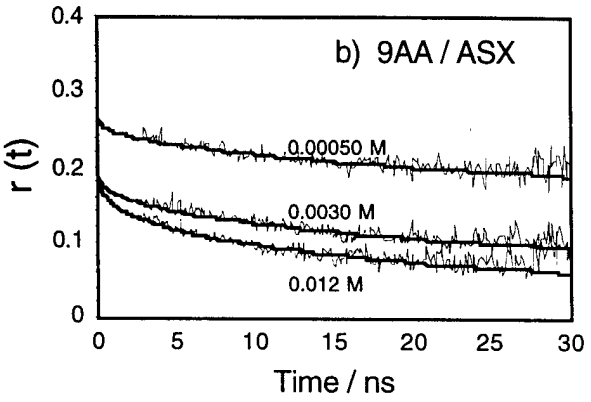

Fig. 1.7b. Time resolved anisotropy *r(t)* decays for 9-aminoacridine doped aluminosilicate xerogels (9AA/ASX) with dopant concentrations of 5.0x10^{-4}, 3.0x10^{-3}, and 1.2x10^{-2} M. The solid curves are calculated fits of the data.

Time Resolved Depolarization Spectra. Representative polarization anisotropy decays for a 9AA/SX glass are shown in Fig. 1.7a. At the lowest 9AA concentration in SX, the depolarization decay is very slow, indicating that the rotational diffusion contribution to the anisotropy decay is nearly negligible for this system, and that it is not significant at higher concentrations. The time-resolved depolarization of the fluorescence emission was obtained by independently measuring the emission polarized parallel $I_{\parallel}$ and the perpendicular $I_{\perp}$ relative to the excitation polarization. The resulting time-resolved anisotropy decay *r(t)* was determined from $I_{\parallel}$ and $I_{\perp}$. Anisotropy decays for 9AA doped SX and ASX are shown in **Fig. 1.7**. The fluorescence depolarization rate clearly increases with increasing 9AA concentration in each matrix. The smooth curves through the data were obtained by: 1) assuming a simple spatial chromophore distribution for *u(r)*.

Excluded volume within the xerogel matrix. The solid lines in Figs 1.8 & 1.9 are best fits to the low concentration energy transfer data (i.e. in the absence of trapping), which yields a dynamic critical radius value of R_0 = 3.2 nm. This value is significantly larger than the static critical radius determined from the spectral overlap integral of the absorption and emission spectra (i.e. R_0 = 2.6 nm), as indicted by the dashed lines. The discrepancy indicates that the bulk concentration does not accurately represent the local chromophore concentration. Furthermore, the larger value for the dynamic critical radius indicates that the 9AA chromophores are significantly excluded from a major fraction of the volume of the bulk glass (i.e. the local concentration is greater than that of the bulk

glass). In addition, since the 9AA chromophore is more soluble in alcohol than in the sol-gel monomer fluid, the chromophores are expected to reside primarily within the pores of the resulting dry xerogel. For 9AA doped SX and ASX the difference between the dynamic and static values for the critical radius indicates that the chromophores are confined to a volume less than 55% of the bulk volume. The 9AA chromophores are confined to a fraction of the total bulk volume in both the SX and ASX porous matrices, resulting in a local concentration than that is higher than for the bulk material.

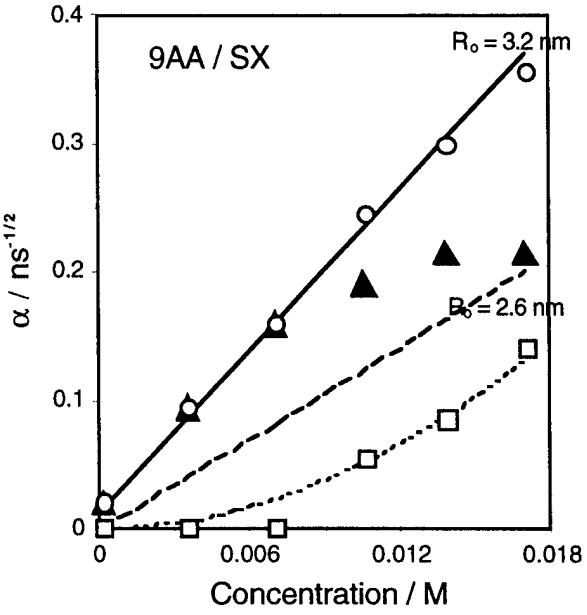

Fig. 1.8. Energy transfer and energy trapping results for 9AA doped silicate xerogels (SX). The donor–donor α_{DD} (Δ) and donor–trap α_{DT} (□) energy transfer parameters are plotted versus the bulk molar concentration of 9AA in the xerogel glass. The solid line is a fit to the low concentration dependence of the donor-donor energy transfer parameter (i.e. in the absence of trapping), corresponding to a dynamic critical radius R_o = 3.2 nm. The dashed line was generated using the static critical radius value R_o = 2.6 nm obtained from the spectral overlap integral. The dotted curve through the energy trapping data (□) is $\alpha_{DT} = 484\ ns^{-1/2}M^{-2} \cdot [9AA]^2$, suggesting the formation of dimer trap species. The sum of the energy transfer and energy trapping parameters $\alpha_{TOT}=\alpha_{DD}+\alpha_{DT}$ (o) increases nearly linearly with concentration.

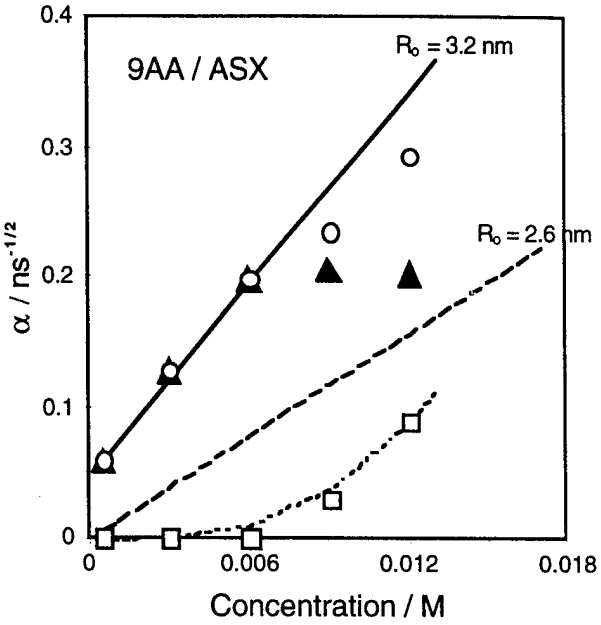

Fig. 1.9. Energy transfer and energy trapping results for 9AA doped aluminosilicate xerogels (ASX). The donor–donor α_{DD} (Δ) and donor–trap α_{DT} (□) energy transfer parameters are plotted versus the bulk molar concentration of 9AA in the xerogel glass. The solid line is a fit to the low concentration dependence of the donor-donor energy transfer parameter (i.e. in the absence of trapping), corresponding to a dynamic critical radius R_o = 3.2 nm. The dashed line was generated using the static critical radius value R_o = 2.6 nm obtained from the spectral overlap integral. The dotted curve through the energy trapping data (□) is $\alpha_{DT} = 5.2\text{x}10^4\ ns^{-1/2}M^{-3} \cdot [9AA]^3$, suggesting the formation of aggregate trap species. The sum of the energy transfer and energy trapping parameters $\alpha_{TOT}=\alpha_{DD}+\alpha_{DT}$, is also shown (o).

1.1 Chromophore Distributions within a Sol-Gel Matrix

Where spatial disorder exists, the probability P(t) that the excitation remains on the originally excited molecule at time t, can be obtained for an arbitrary spatial distribution of chromophores u(r),[25,26]

$$\ln P(t) = -(\rho/\lambda) \int_0^\infty (1-\exp(-\lambda\omega t))\, u(r)d\mathbf{r}$$

where ρ is the number density of chromophores, $u(r)d\mathbf{r}$ is the probability that a chromophore is located a distance r from any initially excited donor chromophore, and λ parametrizes donor-trap (λ=1) and donor-donor (λ=2) energy transfer mechanisms. Thus, an experimental measurement of P(t) can be used to evaluate a trial spatial distribution function u(r).

In an isotropic three dimensional solid (i.e. $u(r)d\mathbf{r} = 4\pi r^2 dr$), the probability that an initially excited donor molecule remains excited a time t after excitation reduces to,[25,34]

$$P(t) = \exp(-\alpha t^{1/2})$$

where $$\alpha = c\,\gamma\,\Gamma(1/2)\,(\lambda\tau_{fl})^{-1/2}$$

and where c is a dimensionless concentration corresponding to the number of chromophores in a sphere of radius R_0 [25]. For chromophores randomly distributed within a restricted geometry such as a zeolite or a bilayer, the time dependence of P(t) can be of a reduced exponent,

$$P(t) \approx \exp(-\beta t^{D/6})$$

where D corresponds to the dimensionality of the restricted lattice and where β characterizes the energy transfer rate.[25][34,35] Thus, the time-dependence of P(t) resulting from energy transfer processes has provided a method for determining the spatial configuration of chromophores in a variety of well defined restricted geometries such as fractal lattices, finite spheres, and polymer chains.[24]

Time-resolved fluorescence depolarization measurements have been used to probe both the spatial distribution of dopant as well as the rates of electronic energy transfer in these novel solids. At high concentrations our depolarization results for quinizarin doped silicate glasses consisted of a fast unresolved component and a slowly decaying component to the fluorescence anisotropy. For the silicate glasses the depolarization results are fit by a spatial distribution consisting of a number of closely spaced neighbors in addition to an underlying random distribution. This suggests that some of the micropores within the xerogel solid appear to be multiply occupied by quinizarin molecules at high concentration. [36]

1.2. Dispersive Energy Transfer in Low Temperature Glasses

Dispersive (i.e. frequency dependent) energy transfer [37] is observed in low temperature glasses and in glasses doped with multiple chromophores due to donor-trap processes. Such mechanisms are important for applications utilizing a light absorbing donor chromophore as an antenna and an optical trap as an actuator. Quinizarin doped aluminosilicate glasses have little dispersion in the optical energy transfer rate at room temperature, however, dispersion is observed at 77K, as shown in Fig. 1.10 [38]. Energy transfer rates for 0.005M Q doped aluminosilica decrease as the excitation wavelength is moved to the red. The nearly dispersionless energy transfer results observed for Q/ASX at room temperature is attributed to significant vibronic contributions to the absorption lineshape, which increases the relative importance of donor-donor processes. [38] A more detailed understanding of inhomogeneous and homogeneous effects is needed to better interpret the different energy transfer dynamics observed in organic versus inorganic polymer matrices.

Porous glasses provide a unique local environment for organic dopants, leading to unique homogeneous linewidths and spectral diffusion dynamics [39]. In addition, the temperature dependent homogeneous dephasing of quinizarin (Q) doped silica sol-gel glasses [40], and of quinizarin adsorbed onto aluminum-oxide powders [41], yield very different dynamics compared with quinizarin doped ethanol glasses [42]. Persistent spectral holes have been observed at high temperature (relative to ethanol glasses [42]) in both quinizarin doped silica xerogels and quinizarin adsorbed onto alumina

(e.g., Q/silica xerogel at 30K [40], and Q/Al_2O_3 powder at 77K [43]). These results have been attributed to reduced electron-phonon coupling of the chromophore to the host matrix.

Time-resolved fluorescence depolarization measurements at different excitation energies have been used to probe dispersive intermolecular optical energy transfer in a quinizarin (Q) doped porous aluminosilica xerogel glass. Optical energy transfer in this system is nearly independent of excitation energy at room temperature. At low temperature, dispersive energy transfer can occur if the homogeneous linewidth is narrower than the inhomogeneous absorption band. Since the lower energy "trap" chromophores are chemically identical to the excited donor molecules, the fluorescence anisotropy decay probes a combination of donor-donor and donor–trap energy transfer processes. Following the model of Stein et. al.[44], the competition between donor–donor (D→D) and donor–trap (D→T) processes is used to evaluate optical energy transfer in a sol-gel matrix.

Previous studies of doped organic polymers (e.g., naphthalene in PMMA) have shown that chromophores covalently linked to a host polymer chain can yield a larger inhomogeneous linewidth than chromophores dissolved within the polymer matrix [44]. For example, the inhomogeneous linewidth for naphthalene chromophores in a PMMA polymer matrix at 65K is nearly 50% larger when the naphthalene molecules are covalently bound to the polymer backbone ($300cm^{-1}$) versus dissolved in PMMA ($215cm^{-1}$). [44] Similarly, when quinizarin is bound to the aluminosilica matrix we observe an inhomogeneous width (at 77 K) of 690 cm^{-1} versus 330 cm^{-1} for the quinizarin-aluminum complex dissolved in an ethanol glass at 77 K (not shown). The larger inhomogeneous broadening observed for chromophores *covalently* bound to polymer matrices has been attributed to the greater tendency for these chromophores to be trapped in unfavorable configurations [44].

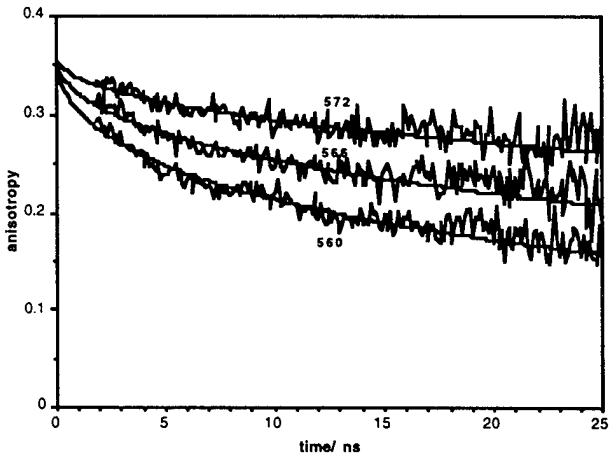

Fig. 1.10. Dispersive energy transfer in Quinizarin doped aluminosilica at 77K. Increased energy transfer is observed as the excitation wavelength is lowered from 572, to 566, and 560nm.

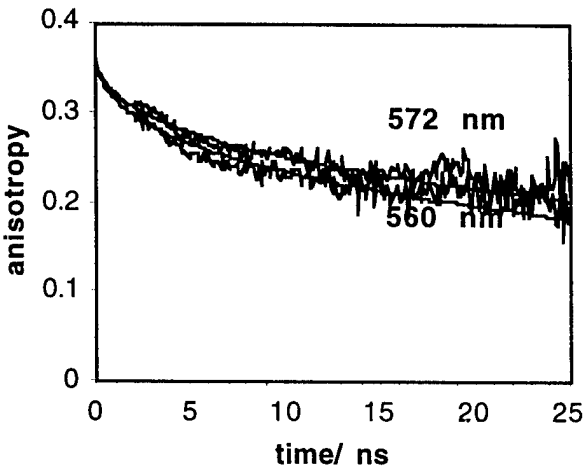

Fig. 1.11. The time-resolved fluorescence anisotropy decays for Q in aluminosilica at 300 K. There is little dispersive energy transfer at room temperature.

Time-resolved fluorescence anisotropy decays for a Q doped aluminosilica xerogel (Q/ASX) at low temperature (77 K) at three different excitation wavelengths (560, 566, and 572 nm) are shown in fig. 1.10. The fluorescence anisotropy decay rate for Q/ASX at low temperature is observed to decrease with increasing excitation wavelength. Energy transfer and trapping at low temperature is restricted to chromophores with an transition energy equal to or lower than the energy of the optically excited species. Thus, chromophores on the red edge of the absorption band yield slower energy transfer rates at low temperature, due to the smaller number of lower energy traps. The energy transfer

parameters predicted using a simplified application of the model of Stein et. al. [44] are compared with the experimental fluorescence depolarization data. The simple (no adjustable parameter) model yields an energy transfer parameter that qualitatively accounts for the dispersion in the low temperature depolarization results.

The time-resolved anisotropy decays for Q/ASX at 300 K are shown in fig. 1.11. The electronic energy transfer rate in Q/ASX at 300K is not as strongly wavelength-dependent, indicating that homogeneous broadening and vibronic contributions to the absorption linewidth are large enough to minimize donor-trap processes at room temperature. In contrast, dispersive energy transfer at room temperature has been reported for naphthalene chromophores covalently linked to a PMMA matrix [44]. The different room temperature energy transfer dynamics observed for naphthalene bound to PMMA versus Q/ASX suggests that homogeneous broadening and vibronic contributions are greater in the Q/ASX absorption spectrum.

2. Local Structure of Porous Sol-Gel Glasses

2.1. Neutron Diffraction Measurements

Small Angle Neutron Scattering (SANS) measurements were performed at the Intense Pulsed Neutron Source (IPNS) at Argonne National Laboratory as a means of probing the pore size distributions in silica and aluminosilica sol-gel glasses. These (not yet published) results provide an independent structural probe of the porous nature of xerogel glasses produced with different chemical protocols (e.g. pH dependent silica xerogels).

Quasi-Elastic Neutron Scattering (QENS) results were also obtained as a measure of the dynamics of organic molecules (e.g. methane) trapped within porous xerogel glasses (not yet published).

2.2. Gas Adsorption Isotherm Measurements of Surface Area

Gas adsorption isotherm measurements (not yet published) have been performed as an independent measure of the effective surface area of porous xerogels. For application of xerogels to chemical sensing applications the interconnectivity of the pores is important for the diffusion of analyte species.

3. Photon Echo Measurements of Homogeneous Dephasing in Sol-Gel Glasses

Temperature dependent (1.2 - 2.1 K) photon echo measurements have been performed on doped aluminosilica sol-gel glasses and organic polymers. In **fig. 3.1** we observe a temperature dependent homogeneous linewidth for both quinizarin and rhodamine in the aluminosilica xerogel (ASX) matrix proportional to T^2, in contrast to the $T^{1.3\pm0.1}$ linewidth dependence typically observed for a variety of organic and inorganic glass hosts in this temperature range (including rhodamine 101 doped PMMA). Even though the chromophore matrix interactions are very different for the covalently bound quinizarin and the ionic dye rhodamine 101 perchlorate, both systems yielded a T^2 dependence of the pure homogeneous dephasing rate versus temperature.

The interest in the optical dephasing of impurities in amorphous solids is fueled by the unusual temperature dependent linewidths relative to doped crystalline systems. For the most part, the anomalous temperature dependent properties observed in glasses have been attributed to the existence of tunneling two-level systems (TLS) [45], and although a void space model has been suggested [46], a physical description of the TLS remains elusive. Temperature dependent homogeneous dephasing measurements of doped porous aluminosilica sol-gel matrices are being used to evaluate the effect of porosity on the low temperature dynamics of the matrix.

Temperature dependent photon echo spectroscopy provides a sensitive probe of how organic chromophores interact with the dynamics of inorganic sol-gel hosts.[47-49] A distribution of two-level systems (TLSs) is often used to model the local fluctuations inherent to a non-equilibrium glassy environment. In addition, temperature dependent photon echo measurements on doped glasses can be

used to probe the dynamics of the TLSs as well as other low frequency modes of the host glass. For example, the thermally induced homogeneous dephasing rate for a doped glass can be given by,[50]

$$1/T_2^* = aT^{\alpha} + be^{-\Delta E/kT}/(1- e^{-\Delta E/kT})$$

The power law term is due to coupling of the optical transition dipole to the TLSs, and the exponential activation term arises from an optical phonon mode of the glass of energy ΔE. [51,52] The temperature dependent exponent α is often related to the TLS density of states by,

$$\rho = \rho_o E^{\mu}$$

where E is the tunnel state splitting, and where $\alpha = 1+\mu$. [53][54].

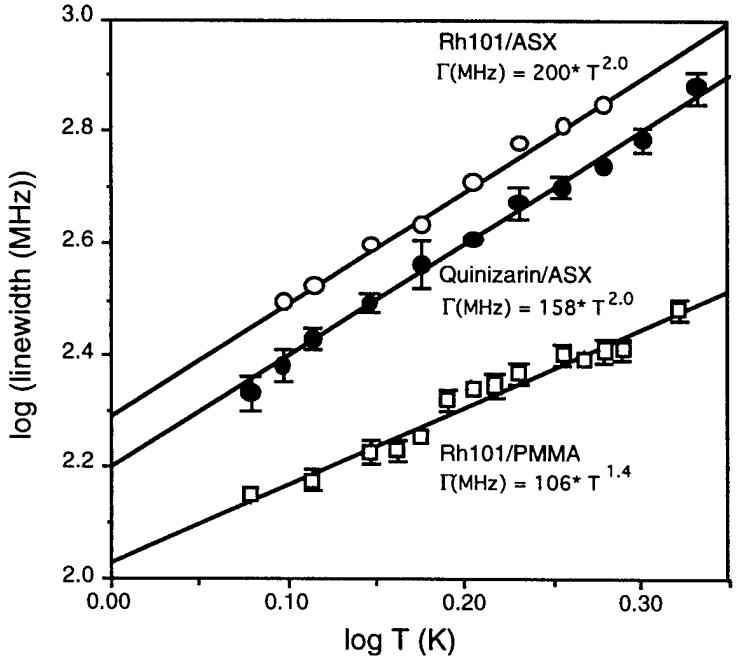

Fig. 3.1. A log-log plot of the temperature dependent linewidth for quinizarin doped aluminosilica xerogel (ASX) (●); rhodamine 101 (Rh101) doped ASX (O); and Rh101 doped PMMA (□). The average value of several measurements are shown with error bars corresponding to ± one standard deviation.

Silica vs. aluminosilica xerogel matrices. The present photon echo results for quinizarin doped aluminosilica [55] can be contrasted with previous spectral hole-burning results on doped silica sol-gel glasses. The low temperature linewidth of several other chromophores in silica sol-gel glasses have been reported to be similar to the $T^{1.3}$ dependence typically observed in organic polymers [56]. In contrast, the present study yields a T^2 linewidth dependence for both Rh101 and quinizarin in ASX. Optical probe [57] and diffraction studies [58] indicate that the aluminosilica xerogel can be more porous than the corresponding acid catalyzed silica xerogel. These structural differences may lead to different TLS dynamics.

Chromophore matrix interactions in an aluminosilica xerogel. Since quinizarin is complexed to aluminum in the ASX matrix, one would expect a stronger coupling to the aluminosilica polymer backbone. Furthermore, since the larger inhomogeneous widths observed for covalently bound polymer chromophores have been attributed to trapping of such chromophores in unfavorable configurations [59], one would expect the quinizarin chromophore in ASX to have a larger distribution of unfavorable configurations [60]. Our observation of a T^2 dependence for the dephasing of both

quinizarin bound to the ASX matrix and for Rh101 in ASX indicates that neither the strength of the coupling to the matrix, nor the inhomogeneous width, is important in determining the nature of the temperature dependent dephasing.

Inorganic sol-gel xerogels vs. organic polymers. A comparison of the photon echo results for Rh101 in ASX versus PMMA indicate that the linewidth of Rh101 in ASX is about twice that for PMMA. This result is similar to the larger homogeneous widths reported for chlorin, oxazine-4 perchlorate, and cresylviolet perchlorate in a silica sol-gel matrix compared with a polyvinyl-butyral polymer host [56]. Both of these studies indicate that the homogeneous dephasing prefactor is larger in the sol-gel matrices versus organic polymer hosts, suggesting a stronger coupling of the chromophores to the sol-gel matrix.

4. Fast Response Optical Limiting in Doped Sol-Gel Glasses

Optical limiting materials are of interest in the design of protective devices for optically sensitive instruments [61] and an important feature of such devices is the ability to create a fast absorbance increase on a sub-nanosecond time scale. We have investigated the mechanisms and time-response of the optical limiting of CAP and the effect of a sol-gel matrix on this process by comparing results for CAP in solution to those for CAP-doped tetraethoxysilane (TEOS) glasses [62b].

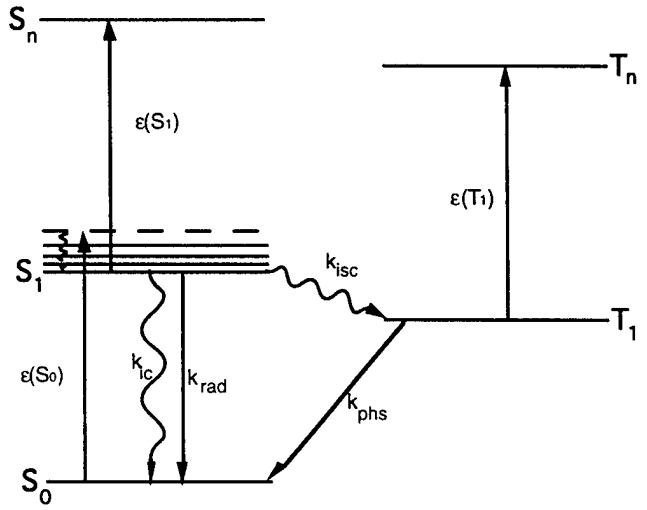

Fig. 4.1. A five-level Jablonski diagram used to describe the fast optical limiting behavior for CAP. For CAP in ethanol the ε and k parameters are listed in Table 1.

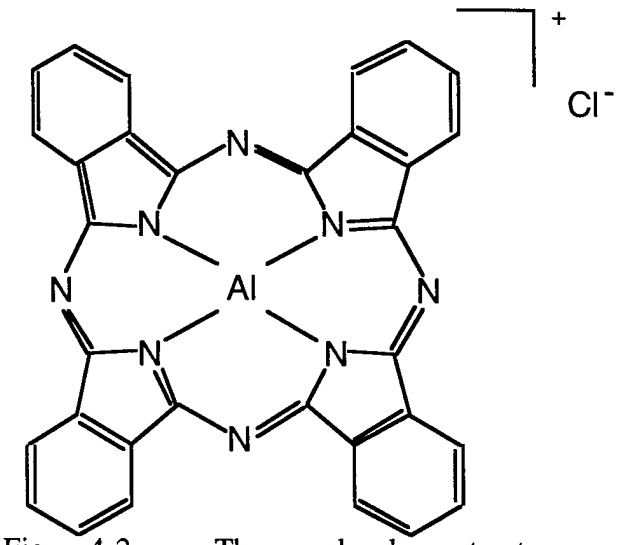

Fig. 4.2. The molecular structure of chloroaluminum-phthalocyanine. CAP ($C_{32}H_{16}N_8AlCl$) has a molecular weight of 574.96 g/mol. and in solution forms a singly charged planar species.

Excited state singlet-singlet absorption processes are found to be responsible for the fast response characteristics (ps to ns) for CAP doped xerogel glasses. Subsequent inter-system crossing and triplet-triplet absorption processes are responsible for the persistent absorbance (ns to ms) determined by the ISC rate and the phosphorescent lifetime of CAP. Inhomogeneous spectral broadening of CAP in the xerogel matrix relative to alcohol solutions was found to have a significant effect on the relative linear (i.e. ground state) versus non-linear (i.e. optically induced excited state) absorption processes. In addition, the faster absorption recovery observed for CAP in a silica xerogel relative to ethanol solution was attributed to an increased rate of electronic to vibrational internal conversion in the xerogel matrix.

Using a picosecond pump-probe optical absorption setup, this work has quantified the photophysical dynamics responsible for the optical limiting behavior of CAP in solution and in a TEOS

sol-gel glass matrix (i.e. the relative contribution and decay parameters associated with S_o->S_1, S_1->S_n and T_1->T_n absorption processes). The optical limiting response time of a CAP doped TEOS sol-gel glass was found to be faster than the 160 ps resolution of the measurement. Furthermore, the dynamic optical limiting behavior of CAP in TEOS revealed a fast relaxation process which was modeled by an increase in internal conversion in the TEOS glass matrix relative to that for CAP in ethanol.

The absorption spectrum of CAP changes considerably upon gelation and drying of the a silica sol-gel host. The absorption spectrum of CAP in ethanol is given in Fig. 4.3. The CAP absorption spectrum in buffered silicate solution resembles that in ethanol, but the spectrum broadens after solvent evaporation.

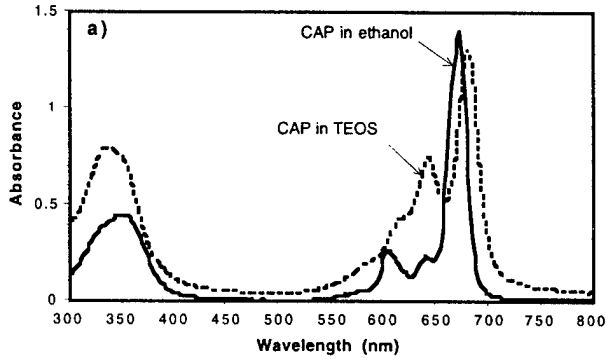

Fig. 4.3a. Comparison of the low intensity absorbance spectra of CAP in ethanol and TEOS. The absorbance at 532 nm is near a minimum. [CAP (in EtOH)] = 1.3×10^{-5} M (path length = 1 cm) and [CAP (in TEOS)] = 1.5×10^{-4} M (path length = 0.2 cm).

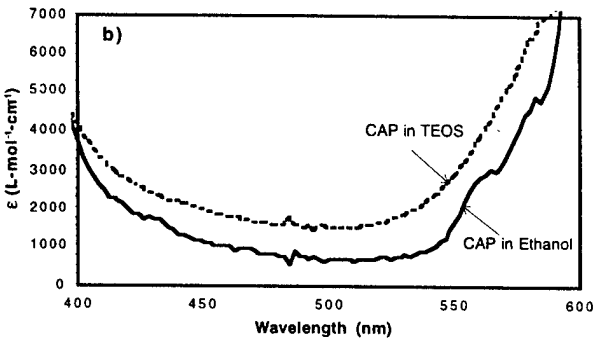

Fig. 4.3b. The ground state extinction coefficient ε_{S0} vs. wavelength for CAP in ethanol versus TEOS obtained using eq (1). Spectral broadening for CAP in the TEOS glass leads to a value of ε_{S0}(532 nm)=2000 L/mol-cm, as compared to ε_{S0}(532 nm)=764 L/mol-cm for CAP in ethanol.

One mechanism used to explain optical limiting involves a nonlinear process in which two rapid, single photon absorptions occur [61-65]. The first absorption corresponds to a relatively weak ground state to excited state transition followed by a second stronger excited state to excited state transition, as illustrated in the Jablonski diagram in fig. 4.1. The first absorption process corresponds to the transition from the ground singlet state (S_0) into the first excited singlet state (S_1). For CAP, this absorption is weak and is characterized by a low extinction coefficient, ε_{So}. The second absorption can involve a transition out of the S_1 state into some higher lying singlet state, S_1->S_n. Alternatively, if enough time has passed to allow intersystem crossing to occur, the second absorption may involve a T_1->T_n transition. In either case, for CAP the excited state transition is found to be much stronger than the S_0 to S_1 absorbance and is characterized by a larger ε value. In general, optical limiting is enhanced when the excited state absorption cross section becomes large relative to that of the ground state, i.e.

$$\frac{\varepsilon_{ex}}{\varepsilon_{S_o}} >> 1$$

For optical limiting based on excited state singlet absorption processes (i.e. S_1 - S_n) the response time is nearly instantaneous. On the other hand, optical limiting behavior based on T_1 - T_n absorbance processes will exhibit a "turn on" time corresponding to the time it takes for the T_1 state to be populated through intersystem crossing from the S_1 level. For CAP in ethanol the intersystem

crossing is t_{isc}=16ns and the fluorescence lifetime is t_{fl} = 6 ns. Thus, optical limiting for CAP in ethanol at short times (≈ 1 ns or less) should be dominated by S_1 - S_n transitions, while if the T_1 - T_n extinction coefficients are significant, T_1 - T_n processes should be the dominant optical limiting mechanism at times greater than the fluorescence lifetime [66,67].

The time-resolved absorbance change caused by optical limiting for a solution of CAP in ethanol is faster than the ~160 ps instrument response, and is therefore much faster than intersystem crossing time (t_{isc}~16ns) required to populate a triplet level. This result confirms that S_1-S_n absorption processes are responsible for the fast response time of the optical limiting dynamics of CAP in ethanol.

A kinetic model was used to determine the relative importance of singlet-singlet and triplet-triplet excited state absorption contributions to the time-resolved optical limiting behavior of CAP. The five-level model illustrated in fig. 4.1 was utilized. The model assumes that the pump pulse creates an initial concentration of photoexcited S_1 states $[S_1]_0$ which then relax to the S_o and T_1 levels. The resulting time-dependent populations of the S_o, S_1, and T_1 levels are,

$$[S_1] = [S_1]_0 \exp[-k_{fl}t]$$

$$[T_1] = \left(\frac{k_{isc}[S_1]_o}{k_{fl} - k_{phos}}\right)\left(\exp[-k_{phos}t] - \exp[-k_{fl}t]\right).$$

$$[S_0] = [CAP] - [S_1] - [T_1]$$

where $[S_1]_0$ is the initial concentration of the photoexcited S_1 state and [CAP] is the total CAP concentration.

Given the time-dependent populations and the corresponding extinction coefficients (ε_{S1}, ε_{T1}, ε_{So}) one obtains the time-dependent absorbance due to both excited state S_1->S_n and T_1->T_n, and ground state S_o->S_1 absorption processes following optical excitation of S_1.

$$A_{ex} = b\left(\varepsilon_{S1}[S_1] + \varepsilon_{T1}[T_1] + \varepsilon_{S0}[S_0]\right)$$

or

$$\Delta A = b\left\{(\varepsilon_{S1} - \varepsilon_{S0})[S_1] + (\varepsilon_{T1} - \varepsilon_{S0})[T_1]\right\}$$

where ΔA is the absorbance change due to optical excitation, i.e. $\Delta A = A_{ex} - A_{unex}$.

CAP doped into a TEOS glass matrix. The low intensity absorption spectrum shown in fig. 4.3b shows that ε_{S0} for CAP in a TEOS glass is more than double the corresponding value for CAP in ethanol. For CAP in TEOS, the ground state extinction coefficient was found to be ≈ 2000 L/mol-cm versus ε_{S0} ≈ 769 L/mol-cm for CAP in ethanol solution. This larger ε_{S0} value decreases the ratio of $\varepsilon_{S1}/\varepsilon_{S0}$ and $\varepsilon_{T1}/\varepsilon_{S0}$, which leads to less efficient optical limiting for the TEOS glass. A comparison of the time-resolved absorbance changes for CAP in ethanol versus CAP doped in a TEOS glass under similar experimental conditions is shown in fig. 4.5a. The optically induced absorbance change for CAP in TEOS is observed to be about four times weaker than that for CAP in an ethanol solution (for equivalent optical densities and under the same excitation conditions). Although the magnitude of the optical limiting for CAP doped into a TEOS glass is less than that for CAP in ethanol under the same excitation conditions, increased optical limiting can be obtained by increasing the optical pump intensity [62,63]. The absorbance change for CAP in TEOS also shows a sharp absorbance increase during optical pumping (near t = 0) that decays on a relatively fast time-scale (i.e. < ns).

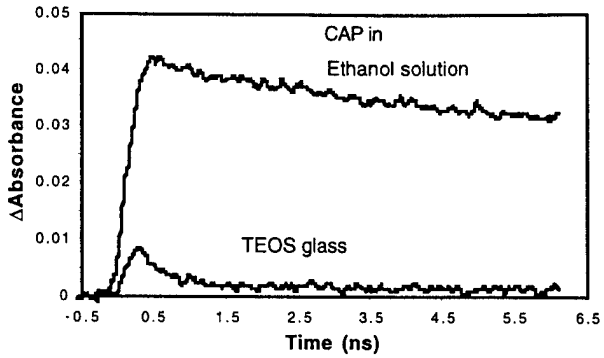

Fig. 4.5a. The optically induced absorbance for CAP in TEOS versus ethanol. Pump energy 2.2 μJ/pulse focused to 60 μm diam. (78 mJ/cm^2). [CAP in EtOH] = 1.0×10^{-3} M with a 1 mm path length, and [CAP in TEOS] ≈ 1.5×10^{-3} M with a 2 mm path length. The reduced magnitude of optical limiting for CAP in TEOS is attributed to a smaller ratio of the excited state and ground state absorption cross sections.

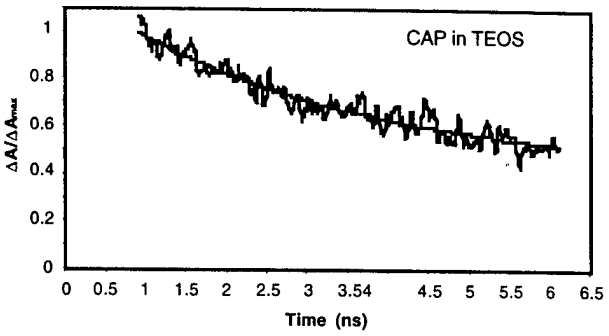

Fig. 4.5b. Kinetic model fit of the normalized sol-gel data. The faster decay kinetics are attributed to an increased internal conversion rate in TEOS (e.g. an increase in k_{isc}). The fit returned a value for k_{ic} of 1.3×10^8 s^{-1}.

A reasonable fit of the model to the CAP/TEOS data was obtained by varying only the value of k_{ic} (relative to the values for CAP in ethanol), as shown in fig. 4.5b. The best fit value for k_{ic} was found to be k_{ic}(CAP/TEOS) = 3.2×10^6 s^{-1} versus a value of k_{ic}(CAP/ethanol) = 1.3×10^8 s^{-1}. This change should correspond to a decrease in the CAP singlet state lifetime from 6.3 ns in ethanol to ≈ 3.5 ns in TEOS, which has been qualitatively confirmed by transient grating measurements [68].

5. Sol-Gel Clad Fiber Optic Chemical Sensors with Time-Resolved Detection

Sol-gel clad fiber optic waveguides have been demonstrated as intrinsic distributed fiber optic chemical sensors [69]. The porous sol-gel cladding allows diffusion of analytes into the evanescent field region close to the fiber optic core. Pulsed optical excitation (0.5 ns) and time-resolved emission detection has been used to simultaneously monitor several multiplexed sensor clad regions along a single optical fiber. Time-resolved detection is also demonstrated as a means of resolving both the spatial location and fluorescence kinetics of intrinsic sensor chromophores along the fiber optic waveguide. Narrow band excitation and spectrally resolved emission provide additional experimental means for discriminating between specific sensor clad regions. A fluorescein doped silica xerogel clad pH sensor and an undoped aluminosilica xerogel clad quinone sensor are demonstrated as intrinsic sol-gel clad fiber optic sensors. The time-resolved fluorescence detection method presented in this study provides a simple method for simultaneously monitoring the spectral changes, spatial location, and kinetic changes associated with a distribution of separate intrinsic fiber optic sensor regions.

Pulsed evanescent excitation and time-resolved detection has been demonstrated as a technique to simultaneous probe intrinsic sol-gel clad sensor elements distributed along a single fiber optic waveguide. In addition, the temporal delay associated with each emission band is used to spatially resolve the intrinsic fluorophore regions along the fiber. Time-resolved emission has also been used to resolve the emission kinetics for an array of intrinsic sol-gel clad fluorophore regions along the fiber optic waveguide. Frequency selective excitation and/or detection can also be used in conjunction with time-resolved detection to further discriminate or address specific sol-gel clad regions.

Fiber optic chemical sensors provide an efficient and inexpensive method for selective in situ real-time chemical sensing [70-73], and the development of distributed [74] and multiplexed [74,74b] fiber optic sensors is of current interest. Fiber optic chemical sensors utilizing evanescent excitation of

sensor chromophores have been reported for a variety of inorganic, organic, and biological analytes [75-80].

A porous glass matrix greatly increases the sensor surface area and permits diffusion of analytes into the optical excitation region. Sol-gel glass materials have been used as a means of noncovalently incorporate a variety of sensor chromophores into a porous matrix that permits the diffusion of analytes into the matrix [81]. A variety of doped sol-gel glasses have been demonstrated as environmental impurity sensors [82]. A number of sol-gel based sensors utilizing fiber optic waveguides have also been reported [83-86]. For example MacCraith et. al. [84] have reported a pH sensor using evanescent wave excitation of fluorescein doped silica cladding at the distal end of a fiber optic waveguide [84], and an intrinsic sol-gel based fiber optic oxygen sensor has been reported based on oxygen quenching of the luminescence of sol-gel incorporated Ruthenium complexes [85].

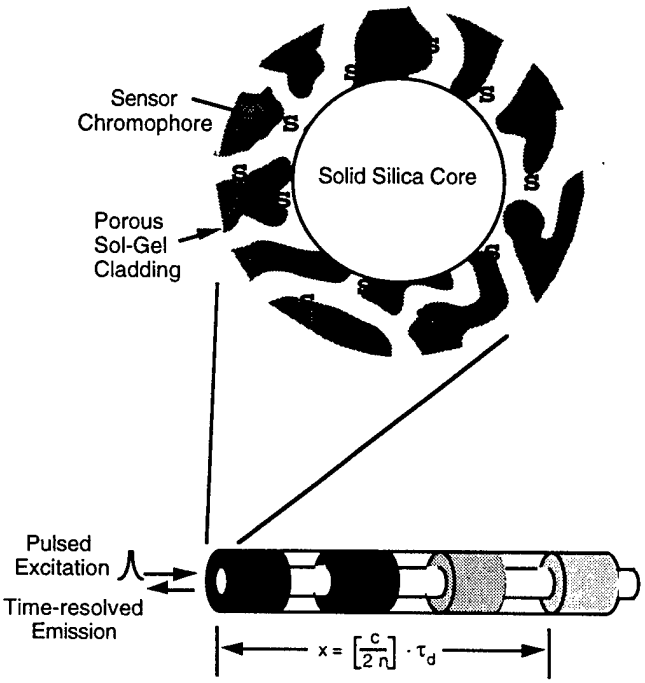

Fig. 5.1. Schematic of a sol-gel clad fiber (not to scale) incorporating sensor molecules (S). The porous matrix and large surface area of the xerogel matrix enhances the number of sensor molecules within the evanescent wave region and allows diffusion of analytes into this region. The fibers utilized in this study consisted of a solid silica core (400μm diameter) with a silicone cladding (50 μm thick) that was locally replaced with fluorophore doped sol-gel clad regions. The ability to spatially resolve the sensor response using pulsed excitation and time-resolved emission detection is also indicated.

Distributed intrinsic sensors: spatial resolution by time-resolved detection. Time-resolved fluorescent detection following pulsed excitation can be used to probe distributed intrinsic fiber optic sensors, resolve fluorophore locations along the fiber, and yield the optical dynamics of the chromophore.

The distance from the fiber front to a fluorophore doped sol-gel clad region is given by,

$$x = \left(\frac{c}{2n}\right) \cdot \tau_d$$

where c is the speed of light in the fiber, n is the index of refraction of the silica core, and t_d is the time delay between the excitation pulse entering and the emission pulse exiting the fiber front. This provides a simple manner for distinguishing between different sensor regions of the optical fiber, or alternatively, it can be used to spatially locate a sensor response along a fiber uniformly clad with a particular sol-gel sensor film.

A sketch of a fiber optic waveguide with intrinsic sol-gel clad regions is shown in **fig. 5.1**. A silicone clad multimode (400mm core diameter) silica core fiber optic waveguide was purchased (General Fiber Optics, Inc.). Multiple small sections (~4 cm long) of the silicone cladding were then removed using a commercial silicone remover (McGean-Rohco, Inc.). After stripping, the bare silica

core regions were rinsed with ethanol, a 5% hydrofluoric acid solution, and distilled water. These sections were then coated with a sol-gel film by dip coating [87] into a dye doped sol-gel solution. Cresyl violet 670 perchlorate (CV), 9-aminoacridine hydrochloride hemihydrate (AA), and disodium fluorescein (FL) were used as dopants in the sol-gel solutions used to clad the optical fibers. A single dipcoat yielded a cladding thickness of approximately 1 μm and the processes could be repeated to increase the cladding thickness.

When an excitation pulse wavelength of 424 nm was used to simultaneously excite both the CV and AA doped sol-gel clad regions along a silica core optical fiber, we obtained the upper time-resolved emission trace shown in **fig. 5.3**. Fluorescence emission from all four of the doped sol-gel clad bands are clearly resolved. The reflected signal from the fiber input face provides a convenient reference point for calibrating the subsequent fluorescence emission from the CV and AA doped sol-gel clad fiber regions. The time delay of the different emission pulses correlates with the spatial locations of the corresponding fluorophore doped sol-gel clad regions along the fiber.

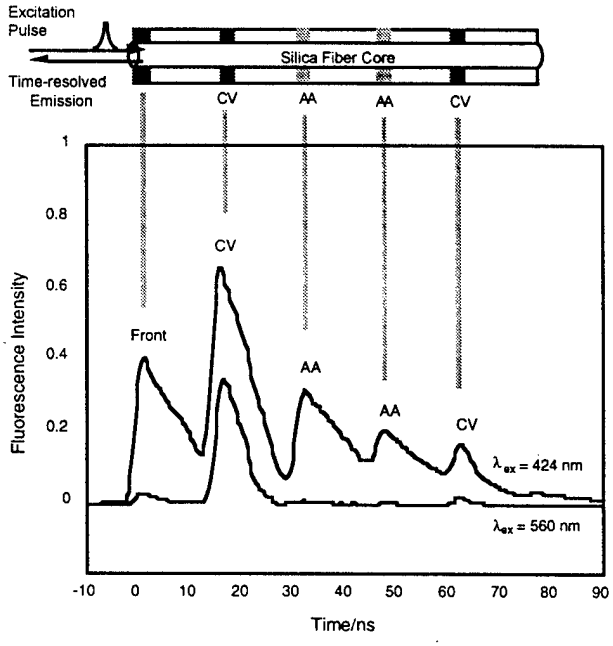

Fig. 5.3. A Time-resolved emission following pulsed laser excitation of the sol-gel clad fiber. Vertical lines correlate different emission signals with fiber cladding regions. The upper trace was obtained with excitation at 424 nm and detection ≥475 nm. In the lowest trace, the emission from AA was selectively reduced by shifting the excitation to the red of AA (e.g. 560 nm).

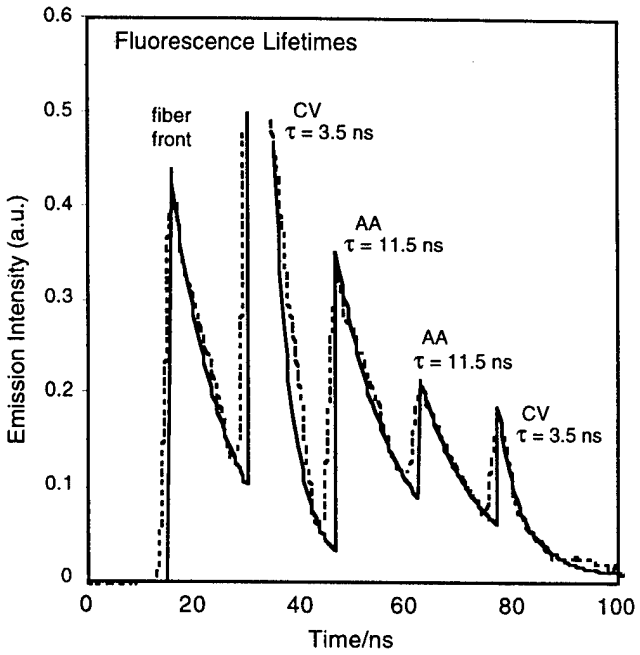

Fig. 5.4. Time-resolved emission from aminoacridine (AA) and cresyl violet (CV) doped sol-gel clad regions distributed along a 9 m long fiber optic waveguide (dashed curve). The solid curve is a least squares fit of the data to a sum of time-offset exponential decays (corresponding to the locations of the fluorophore bands along the fiber).

Fluorophore lifetimes. It is straight forward to extend fiber optic fluorescence lifetime techniques [88] to obtain simultaneous fluorescence lifetime measurements on several intrinsic sol-gel clad fluorophores. The temporal profile of each individual emission band is characteristic of the fluorescence lifetimes of the corresponding fluorophore. Since both the 0.5ns excitation pulse and the optical transit time across a 4cm wide sensor element (0.13ns) are short relative to the fluorescence lifetimes of the chromophores in this study, the time-resolved emission can be used to probe the emission kinetics of the fluorophores, as shown in **fig. 5.4**.

The ability to resolve the fluorophore decay kinetics of a distributed array of intrinsic chromophore regions along the fiber optic indicates that changes in fluorescence kinetics may be used

as an additional variable for detecting the individual responses of a distribution of intrinsic sensors [70,88b]. A sensor device based upon kinetic changes can alleviate sensor degradation and leaching problems, since the emission lifetime is insensitive to chromophore concentration.

Spectral resolution. Selective optical excitation and detection of an integrated array of sensor elements can be also be obtained utilizing tunable narrow band excitation combined with spectrally and temporally resolved emission of multiple chromophore elements, as shown in **fig. 5.3**.

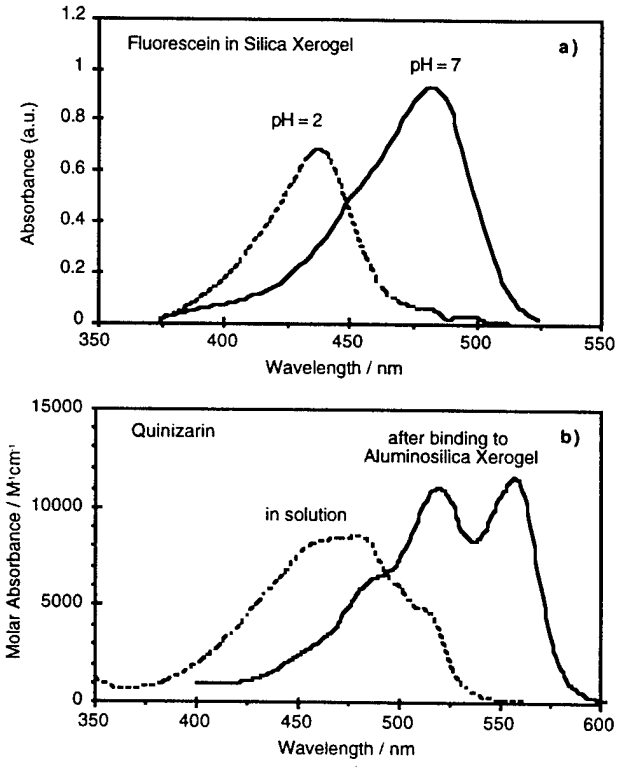

Fig. 5.6. a) The absorption spectrum of fluorescein (FL) in a silica xerogel (SX) at pH = 2 (dashed curve) and pH=7 (solid curve). b) The quinizarin (Q) absorption spectrum shifts to the red upon complexation with aluminum in the ASX matrix. 560 nm excitation wavelength is more strongly absorbed by the Q-Al complex formed as Q binds to the ASX cladding.

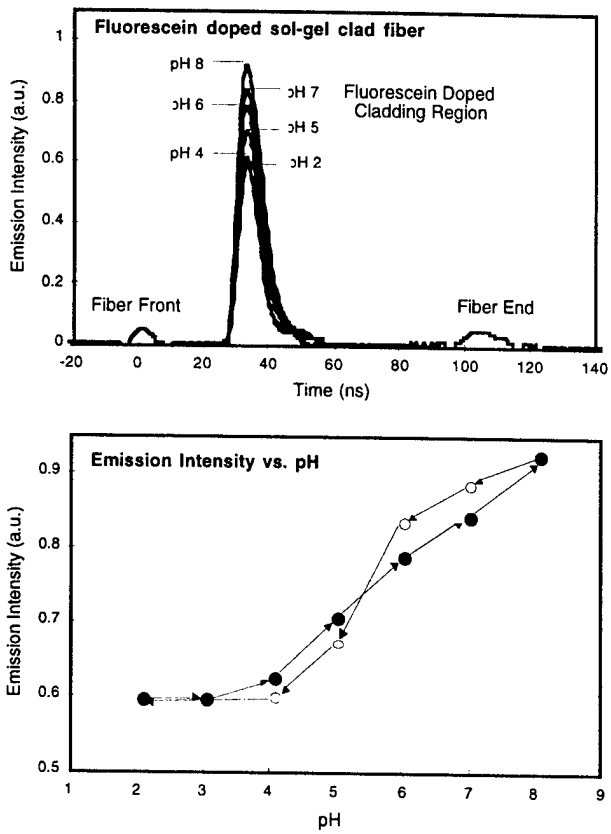

Fig. 5.7. a) Time-resolved emission intensity following pulsed evanescent excitation (at 500 nm) of an intrinsic fluorescein doped sol-gel clad region on a fiber optic waveguide. A decrease in absorption occurs as the pH is lowered. Reflections of the excitation pulse off of the front and distal ends are shown for reference. b) A pH titration curve for the time-resolved fiber optic sensor.

Intrinsic sol-gel clad fiber optic sensors. Time-resolved optical detection of prototypical sol-gel clad fiber optic sensor waveguides have been demonstrated. The porous nature of the xerogel allows diffusion of analyte species into the evanescent field region of the cladding where they can be optically detected. A fluorescein (FL) doped silica xerogel clad fiber and an undoped aluminosilica xerogel clad fiber are demonstrated as intrinsic pH and quinone sensors, respectively.

The absorption maximum of fluorescein (FL) in a porous silica xerogel (SX) shifts from 490 nm in a pH=7 solution to 440 nm when immersed in a pH=2 solution, as shown in **fig. 5.6a**. The large pH induced change in the FL absorption spectrum indicates that protons (and associated ions) are

able to easily diffuse through the porous xerogel matrix. A 7 meter long fiber with a single FL doped sol-gel clad region was utilized as an intrinsic optical fiber pH sensor. Using an excitation wavelength of 500nm, the emission intensity from the FL doped sol-gel clad region was observed to decrease as the pH of the solution surrounding the cladding region was lowered, as shown in **fig. 5.7a**. At lower pH the FL/SX absorbance at 500nm is reduced (as shown in **fig. 5.6a**), resulting in a corresponding decrease in emission intensity. Reflections of the excitation pulse off of both the front and distal ends of the 7 m long fiber are useful reference points. The titration of the time-resolved sensor emission intensity, shown in **fig. 5.7b**, is similar to static spectroscopic studies of FL in solution and doped into silica xerogel monoliths [89].

The pores of the sol-gel matrix are large enough to allow the diffusion of larger organic analytes into the evanescent detection region. An aluminosilica xerogel (ASX) clad region of a fiber optic waveguide was exposed to a 10^{-3} M quinizarin solution, allowing quinizarin (Q) to diffuse into the ASX cladding and irreversibly bind to aluminum in the matrix, forming a Q-Al complex with a distinct spectral signature. The complexation of Q by the ASX matrix was spectroscopically monitored using the absorption origin of the Q absorption spectrum, which shifts from a wavelength of 520 nm to 560 nm upon complexation with Al within the ASX matrix (not shown) [69].

C. Publications Acknowledging ARO Support

1. D. L'Esperance, C. A. Browne, and E. L. Chronister, "Chromophore Dynamics in Sol-Gel Glasses and Xerogel Clad Fiber Optic Sensors," MRS Proceedings: Better Ceramics Through Chemistry VI, vol. 346, A.K. Cheetham Ed. (MRS, Pittsburgh, PA, 1994), pp. 579-584..

2. D. L'Espérance and E. L. Chronister, "Electronic energy transfer and trapping in quinizarin-doped aluminosilicate sol-gel glasses," Chemical Physics Letters, 222 (1994) 217-223.

3. D. L'Espérance and E. L. Chronister, "Dispersive electronic energy transfer in an organically doped xerogel glass," Chemical Physics, 195 (1995) 387-393.

4. S.C. Laperriere, J.W. Mullens, D. L'Espérance, and E. L. Chronister, "Optical energy transfer and trapping in 9-aminoacridine doped sol-gel glasses," Chemical Physics Letters, 243 (1995) 114-124.

5. C.A. Browne, D.H. Tarrant, M.S. Olteanu, J.W. Mullens, and E. L. Chronister, "Intrinsic Sol-Gel Clad Fiber-Optic Sensors with Time-Resolved Detection," Analytical Chemistry, 68 (1996) 2289-2295.

6. J.J. Flores and E. L. Chronister, "Doped sol-gel materials as a matrix for fast response photochromic devices," SPIE: Smart Materials Technologies, 2716 (1996) 194-204.

D. Participating Scientific Personnel

Principle Investigator:	Eric L. Chronister
Graduate Students:	Drew L'Espérance, Ph.D. 7/93 John Pelo, M.S. 9/94 James Flores, M.S. 6/95 Clarice Browne, M.S. 6/95
Undergraduate Students:	Joseph Mullens John Middleton Marta Olteanu

D2. Advanced Degrees Earned while employed on the project

1. D. L'Espérance, Ph.D., 7/1993,
"Molecular Dynamics and Optical Energy Transfer in Organically Doped Porous Sol-Gel Glasses".

2. J.J. Flores, M.S., 6/1995,
"Spectroscopy of Unique Molecular Solids: Chloro-aluminum-phthalocyanine Photophysics in Porous Xerogel Matrices and Anharmonic Vibrational Behavior of Organic Polymers Under High Pressure".

Bibliography

[1] A. Goetzberger, V. Wittwer, Solar Cells **4** (1981) 3.

[2] A. Hinsch and A. Zastrow, Proc. SPIE **1272**, Optical Materials Technology for Energy Efficiency and Solar Energy Conversion IX (1990) 208-217.

[3] R.Reisfeld, D.Brusilovsky, M.Eyal, E. Miron, Z.Burstein, and J.Ivri Chem. Phys. Lett. **160** (1989) 43-44.

[4] Y.Kobayashi, Y.Kurokawa, Y.Imai, S.Muto J. Non-Cryst. Solids **105** (1988) 198-200.

[5] T. Tani, H. Namikawa, and K. Arai, J. Appl. Phys **58** (1985) 3559-3565.

[6] R. Reisfeld, Proc. SPIE **1328**, Sol-Gel Optics (ed MacKenzie J D & Ulrich D; 1990) 29-39.

[7] H. Dislich, *J. Non-Cryst. Solids* 57 371 (1983)

[8] L. Hench, J. West, B. Zhu, and R. Ochoa, Sol-Gel Optics, edited by J D MacKenzie and D. Ulrich (*Proc. SPIE* 1328 1990) p 230

[9] D. Avnir, D. Levy and R. Reisfeld, J. Phys. Chem. 88 (1984) 5956.

[10] D. Avnir, R. Kaufman, R. Reisfeld, J. Non-Cryst. Solids 74 (1985) 395.

[11] L.L. Hench and J.K. West, Chem. Rev. 90 (1990) 33.

[12] D. Lo, J.E. Parris and J.L. Lawless, Appl. Phys. B 56 (1993) 385.

[13] R. Reisfeld and G. Seybold, J. Lumin. 48&49 (1991) 898.

[14] J. M. McKiernan, S. A. Yamanaka, B. Dunn and J. Zink, J. Phys. Chem., 94 (1990) 5652.

[15] C. Whitehurst, D.J. Shaw and T.A. King, in Sol-gel optics, eds J.D. Mackenzie and D.R. Ulrich, Proc. SPIE 1328 (1990) 183.

[16] A. Hinsch and A. Zastrow, in Optical Materials Technology for Energy Efficiency and Solar Energy Conversion IX, Proc. SPIE 1272 (1990) 208.

[17] R. Reisfeld,D. Shamrakov and C. Jørgensen, Solar Energy Materials and Solar Cells, 33 (1994) 417.

[18] R. Zusman, C. Rottman, M. Ottolenghi and D. Avnir, J. Non-Cryst. Solids, 122 (1990) 107.

[19] M. Brunel, F. Le Luyer, M. Canva, A. Brun, F. Chaput, L. Malier and J.-P. Boilot, Appl. Phys. B 58 (1994) 443.

[20] M. Canva, G. Le Saux, P. Georges, A. Brun, F. Chaput and J.-P. Boillot, Opt. Lett. 17 (1992) 218.

[21] Sol-Gel Optics: Processing and Applications, L.S. Klein, ed., (Kluwer Academic, Boston, 1994)

[22] R. Reisfeld and C.K. Jorgensen, in Structure and Bonding, v 77: Chemistry, Spectroscopy and Applications of Sol-Gel Glasses, R. Reisfeld and C. K. Jorgensen, eds. Spinger-Verlag, Berlin 1992.

[23] R. Reisfeld, in Sol-gel optics, eds J.D. Mackenzie and D.R. Ulrich, Proc. SPIE 1328 (1990) 29.

[24] K. Peterson, A. Stein, and M.D. Fayer, Molecular Dynamics in Restricted Geometries, ed. by J. Klafter and J.M. Drake (Wiley, New York, 1989).

[25] J. Baumann and M.D. Fayer, J. Chem. Phys. 85 (1986) 4087-4107.

[25b] D. L'Espérance, E.L. Chronister, Chemical Physics Letters, 222, 217-223 (1994).

[26] M. Ediger and M.D. Fayer, Macromolecules 16 (1983) 1839-1844.

[27] J. M. Drake, J. Klafter, and P. Levitz, Science, **251,** 1574 (1991)

[28] S.C. Laperrière, J.W. Mullens, D. L'Espérance, E.L. Chronister, Chemical Physics Letters, 243,114-124 (1995).

[29] P. Gangola, N.B. Joshi and D.D. Pant, Chem. Phys. Lett. 80 (1981) 418.

[30] D.D. Pant, G.C. Joshi and H.B. Tripathi, Pramana 27 (1986) 161.

[31] K. Kasama, K. Kikuchi, Y. Nishida and H. Kokubun, J. Phys. Chem. 85 (1981) 4149.

[32] M.D. Barkley, A.A. Kowalczyk and L. Brand, J. Chem. Phys. 75(1981) 3581.

[33] I. Gryczynski, H. Cherek, G. Laczko and J.R. Lacowicz, Chem. Phys. Lett. 135 (1987) 193.

[33b] D. Fornasiero and T. Kurucsev, Chem. Phys. Lett. 117 (1985) 176.

[34] J. Klafter and A. Blumen, J. Chem. Phys. **80** (1984) 875.

[35] Th. Forster, Z. Naturforsch., **A4** (1949) 321.

[36] D. L'Esperance, C.A. Browne, E.L. Chronister, MRS Proceedings: Better Ceramics Through Chemistry VI, vol. 346, A.K. Cheetham Ed. (MRS, Pittsburgh, PA, 1994), pp. 579-584.
[37] M.D. Ediger, M.D. Fayer, J. Phys. Chem. 88 (1984) 6108
[38] D. L'Espérance, E.L. Chronister, Chemical Physics, 195, 387-393 (1995).
[39] R. Locher, A. Renn, and U. P. Wild, Chem. Phys. Lett., 138 (1987) 405
[40] T. Tani, H. Namikawa, K. Arai, and A. Makishima, J. Appl. Phys 58 (1985) 3559
[41] Th. Basché and C. Bräuchle, Chem. Phys. Lett., 181 (1991) 179
[42] J. Friedrich, H. Wolfum, and D. Haarer, J. Chem. Phys. 77 (1982) 2309
[44] A.D. Stein, K.A. Peterson, and M.D. Fayer, J. Chem. Phys. 92 (1990) 5622-5635
[45] W.A. Phillips, Ed., Amorphous Solids: low-temperature properties (Springler-Verlag, Berlin 1981).
[46] M. H. Cohen and G. S. Grest, Phys. Rev. Lett. **45**, 1271 (1980); and Solid State Commun **39**, 143 (1981).
[47] L. Narasimhan, K. Littau, Y. Bai, D. Pack, A. Elschner and M.D. Fayer, *J. Luminescence* 45 (1990) 49-53.
[48] D. Pack, L. Narasimhan, and M.D. Fayer, *J. Chem. Phys.* 92 (1990) 4125-4138.
[49] M. Berg, C. Walsch, L. Narasimhan, K. Littau, M.D. Fayer,*J. Chem. Phys.* 88 (1988) 1564.
[50] B. Jackson and R. Silbey, *Chem. Phys. Lett.* 99 (1983) 331 = [51].
[52] H. Meijers and D. Wiersma, *Chem. Phys. Lett.* 181 (1991) 312-318.
[53] S. K. Lyo in: Electronic Excitation Processes in Organic Molecular Aggregates, Vol **49**, Springer Series in Solid State Sciences, eds. P. Reineker, H. Haken and H. C. Wolf (Springer-Verlag, Berlin, 1983) p215.
[54] R. Jankowiak and G. J. Small, Chem. Phys. Lett. **207**, 436 (1993).
[55] B.J. Baer, E.L. Chronister, Journal of Chemical Physics, 103, 9880-9883 (1995).
[56] R. Locher, A. Renn and U. P. Wild, Chem. Phys. Lett. 138 (1987) 405.
[57] J. McKiernan, J-C Pouxviel, B. Dunn, and J.I. Zink, J. Phys. Chem. **93**, 2129 (1989).
[58] S. Hietala, D. Smith, C. Brinker, A. Hurd, A. Carim, and N. Dando, J. Am. Ceram. Soc. **73**, 2815 (1990).
[59] A.D. Stein, K.A. Peterson, and M.D. Fayer, J. Chem. Phys. **92**, 5622 (1990).
[60] D. L'Espérance and E. L. Chronister, Chem. Phys. **195**, 387 (1995).
[61] L. Tutt and T. Boggess, *Prog. Quant. Electr.* **17**, 299-338, 1993; and
L. Tutt, S. McCahon, M. Klein, *Electro-Optical Materials for Switches, Coatings, Sensor Optics, and Detectors*, SPIE Vol 1307, 315-326, 1990.
[62b] J.J. Flores, E.L. Chronister, Proc SPIE - Smart Materials Technologies, edited by A. Crowson, vol 2716, (1996), 194-204.
[62] F. Bentivanga, M. Canva, P. Georges, A. Brun, F. Chaput, L. Malier, J.-P. Boilot, *Applied Physics Letters* 62, 1721-1723, 1993.
[63] M. Brunel, F. Le Luyer, M. Canva, A. Brun, F. Chaput, L. Malier, J.-P. Boilot, *Applied Physics B* **58**, 443-445, 1994.
[64] D. R. Coulter, V. M. Miskowski, J. W. Perry, T. Wei, E. Van Stryland, D. Hagan, *Materials for Optical Switches, Isolators, and Limiters*, SPIE Vol. **1105**, 42-51, 1989.
[65] J. W. Perry, K. Mansour, S. R. Marder, et. al., *Optics Letters*, **19**, 625-627, 1994.
[66] J. W. Perry, L. R. Khundkar, T. H. Wei, M. J. Sence, *Organic Materials for Nonlinear Optics and Photonics*, J. Messier et. al. (eds.), NATO ASI Series E, **194**, 369-382, 1991.
[67] J. H. Brannon and D. Magde, *Journal of the American Chemical Society*, **102**, 62-65, 1980.
[68] Bruce J. Baer, unpublished transient grating results.
[69] C.A. Browne, D.H. Tarrant, M. Olteanu, J.W. Mullens, E.L. Chronister, Analytical Chemistry, 68, 2289-2295 (1996).
[70] Seitz, W.R. *Anal. Chem.* **1988**, *19*, 135-173.
[71] Barnard, S.; Walt, D. *Environ. Sci. Technol.* **1991**, *25*, 1301-1304.
[72] Moslehi, B.; Shahriari, M.; Schmidlin, E.; Anderson, M.; Lukasiewicz, M. *Laser Focus World*, April **1992**, 161-168.

[73] Arnold, M.A. *Anal. Chem.* **1991**, *64*, 1015 A-1025 A.
[74] SPIE Conference on Optics, Imaging, and Instrumentation, July 24-29, 1994, San Diego CA. Symposia: #2292 "Fiber Optic and Laser Sensors XII"; #2293 "Chemical, Biochemical, and Environmental Fiber Sensors VI"; #2294 "Distributed and Multiplexed Fiber Optic Sensors IV".
[74b] Pantano, P.; Walt, D.R. *Anal. Chem.* **1995**, *67*, 481A-487A.
[75] Hobbs, J.R. *Laser Focus World*, May **1992**, 83-86.
[76] Ge, Z.; Brown, C.W.; Sun, L.; Yang, S.C. *Anal. Chem.* **1993**, *65*, 2335-2338.
[77] Periasamy, N. *Applied Optics* **1982**, *21*, 2693-2695.
[78] Piraud, C.; Mwarania, E.; Wylangowski, G.; Wilkinson, J.; O'Dwyer, K.; Schiffrin, D.J. *Anal. Chem.* **1992**, *64*, 651-655.
[79] Leiberman, R.A.; Blyler, L.L.; Cohen, L.G. *J. Lightwave Technology* **1990**, *8*, 212-220.
[80] Lundgren, J.S.; Bekos, E.J.; Wang, R.; Bright, F.V. *Anal. Chem.* **1994**, *66*, 2433-2440.
[81] Lev., O.; Tsionsky, M.; Rabinovich, L.; Glezer, V.; Sampath, S.; Pankratov; Gun, J. *Anal. Chem.* **1995**, *67*, 22A-30A.
[82] Reisfeld, R. in Sol-Gel Optics, J.D. MacKenzie and D. Ulrich, eds. Proc. SPIE **1990**, *1328*, 29-39.
[83] Grattan, K.T.V.; Badini, G.E.; Palmer, A.W.; Tseung, A.C.C. *Sensors & Actuators A* **1991**, *A26*, 483-487.
[84] MacCraith, B.D.; Ruddy, V.; Potter, C.; O'Kelly, B.; McGilp, J.F. *Electronic Letters* **1991**, *27*, 1247-1248.
[85] MacCraith, B.D.; McDonagh, C.M.; O'Keefe, G.; Keyes, E.T.; Vos, J.G.; O'Kelly, B.; McGilp, J.F. *Analyst* **1993**, *118*, 385-388.
[86] MacCraith, B.D.; McDonagh, C.M.; O'Keefe, G.; McEvoy, A.K.; Butler, T.; Sheridan, F.R.. *Sensors and Actuators* **1995**, *B29*, 51-57.
[87] Dislich, H. *J. Non-Cryst. Solids* **1983**, *57*, 371-388.
[88] Brown, R.S.; Brennan, J.D.; Krull, U.J. *Microchemical Journal*, 1994, *50*, 337-350.
[88b] Thompson, R.B.; Lakowicz, J.R. *Anal. Chem.* 1993, *65*, 853-856.
[89] Shamansky, L.M.; Yang, M.; Olteanu, M.; Chronister, E.L. *Materials Letters* **1996**, *26*, 113-119.